CHAPTER 1

INTRODUCTION AND LITERATURE REVIEW

An antenna is a structure that radiates or receives electromagnetic (EM) waves and therefore it can be used as a transmitting antenna or a receiving antenna. The antenna is an essential and important part of any wireless communication. It acts as a transducer by converting electrical signal to EM waves and vice-versa.

In the wireless communication and radar systems, antenna is the only interfacing device attached to both the transmitter as well as the receiver. Wideband communication systems can provide high data rates, voice biometrics, multi-lingual communication, multiple communication channels, and controlled data traffic due to availability of wide frequency spectrum. Thus, large impedance bandwidth is required for efficient wireless communication and pulse radar systems. A dielectric resonator antenna (DRA) is one of the best options to achieve wide impedance bandwidth [Ullah et al. (2015)].

1.1 Brief History of DRAs

An American physicist, R.D. Richtmyer theoretically predicted that a dielectric piece of suitable shape can function as a microwave resonator and he coined the term "dielectric resonator (DR)" in 1939 [Richtmyer (1939)]. Later in 1962, Okaya and Barash worked on single crystal rutile which possesses high dielectric constant [Okaya (1962a) (1962b)] They first provided the analysis of modes inside the resonator and measured its dielectric constant in the microwave frequency range. In the early 1980s, Long gave an introductory experimental investigation on the resonant cylindrical dielectric cavity antenna [Long et al. (1983)]. After that a lot of work has been carried out by researchers on various types of DRAs which are excited using different feeding mechanisms.

1.2 Important DRA Parameters

In order to elaborate the performance of an antenna, understanding of various parameter is necessary. In reality, there are a number of important parameters which describe the performance of an antenna. For the present research work, the parameters that will be looked at include the return loss, frequency bandwidth, radiation pattern and gain.

1.2.1 Return loss (RL)

In wireless communication, *RL* is defined as the power loss in the signal, which is reflected / received by a discontinuity within a transmission line. This discontinuity can be either a mismatch with a device inserted in the transmission line or with the terminating load. The *RL* is a function of the incident and reflected power, and is given by (1.1).

$$RL\ (\text{dB}) = 10\log\frac{P_i}{P_r} \tag{1.1}$$

where P_i is the incident power and P_r is the reflected power.

In case of antennas, the return loss is the parameter by which it is decided how well the antenna is matched with the rest of the device. High value of return loss indicates good matching between two media. The return loss can be calculated using (1.2).

$$RL = P_i - P_r \tag{1.2}$$

where *RL* is the return loss (dB), P_i is the incident power (dBm) and P_r is the reflected power (dBm).

The ratio of amplitude of reflected wave, V_r to the amplitude of the incident wave, V_i, is called the reflection coefficient, Γ. The reflection coefficient can be given by (1.3)

$$\Gamma = \frac{V_r}{V_i} \tag{1.3}$$

The reflection coefficient can also be expressed in terms of the source impedance and the load impedance. This is given by eq. (1.4).

$$\Gamma = \frac{Z_L - Z_S}{Z_L + Z_S} \tag{1.4}$$

where Z is the load impedance and Z_S is the source impedance.

The magnitude of reflection coefficient $|\Gamma|$ is given by eq. (1.5)

$$|\Gamma| = \frac{\text{VSWR}-1}{\text{VSWR}+1} \tag{1.5}$$

The return loss of an antenna is the negative of reflection coefficient in dB. The relation is given below in eq.(1.6).

$$RL = -20\log_{10}|\Gamma| \text{ dB} \tag{1.6}$$

It can be seen from the foregoing equations that the return loss is related to both VSWR and the reflection coefficient. An increase in return loss corresponds to a decrease in VSWR. The return loss is generally preferred over VSWR because it has a better resolution for lower values of reflection coefficient.

1.2.2 Frequency bandwidth

In antennas, the frequency bandwidth can be taken as the specific range of frequencies on either side of the centre/resonant frequency, within which an antenna performance characteristics are within acceptable values of those at the centre/resonant frequency. From antennas standards, one of the important antenna characteristics is the return loss and its acceptable value is at least 10 dB [Balanis (2005)].

The frequency bandwidth of antennas can be given in terms of either the absolute bandwidth or fractional bandwidth. The absolute bandwidth, *ABW, is* expressed as a difference between the upper and lower limits of the frequency range. It is given by eq. (1.7)

$$ABW = f_H - f_L \tag{1.7}$$

where f_H and f_L are the upper and lower limits respectively of the frequency range at a return loss of 10 dB.

The fractional bandwidth of an antenna is a measure of how wideband the antenna is. If the antenna operates at centre frequency f_c between lower frequency f_L and upper frequency f_H (where $f_c = (f_L + f_H)/2$), then the fractional bandwidth (*FBW)* is given by

$$FBW = \frac{f_H - f_L}{f_c} \tag{1.8}$$

where f_H and f_L are the upper and lower limits respectively of the frequency range at a return loss of 10 dB. The fractional bandwidth varies between 0 and 2, and is often quoted as a percentage (between 0% and 200%). Wideband antennas typically have a FBW of 20% or more. Antennas with a FBW greater than 50% are referred as ultra-wideband antennas.

1.2.3 Bandwidth enhancement techniques for DRAs

Many radar and emerging wireless systems operate over wide frequency range. Therefore, they require broadband antennas for communication. Several methods are used for enhancement of DRA bandwidth. The DRA bandwidth can be enhanced i) using a combination of multi permittivity DRAs, ii) using modified feed configuration, iii) using modified DRA shapes, and iv) using hybrid antennas.

(a) Combination of multi permittivity DRAs: Two or more dielectric resonators (DRs) combined together enhances the bandwidth, either because of reduction in effective dielectric constant or merging of neighbouring mode excited in neighbouring DRs. The foregoing concept is utilized in DRA design by providing air gap between the substrate and DR or between two DRs [Cooper et al. (1996); Liasne et al. (2001)], using annular DRs [Luk and Leung (2003)], providing notch in rectangular DRAs (RDRAs) [Ittipiboon et al. (1996)], using multi-segment DRAs [Petosa et al. (1996) (1997a) (1997b)], co-planar parasitic DRAs [Fan et al. (1996), Sangiovanni et al. (1997)], embedded DRAs [Kishk (2005)], staircase-shaped DRA [Chair et al. (2007) (2006b)], perforated DRAs

[Chair et al. (2006a)], and stepped pyramid DRAs [Chair et al. (2004)] to enhance the impedance bandwidth of DRAs.

(b) Modified feed configuration: The impedance bandwidth can also be increased without significantly affecting other properties of DRAs through modification in conventional feeding techniques or new design of feed i.e. using stub [Luk and Leung (2003)], probe feed with air gap [Luk and Leung (2003)], flat matching strips [Luk et al. (1999); Leung et al. (2000)], ring aperture feed [Leung et al. (1998) (2002); Yung (1998)], U-shaped aperture feed [Li et al. (2005)] or multi-mode generation through composite excitation [Petosa (2007)].

(c) Modified DRA shapes: Impedance bandwidth of conventional DRAs can also be improved by modifying the shape of DRs. Modified shape either generates different mode/ combination of neighbouring modes or reduces diffraction from the edges which results in the increase of DRA bandwidth. Some of the modified shapes are conical and inverted split conical DRAs [Kishk et al. (2001a) (2001b)], tetrahedral and inverted tetrahedral DRAs [Kishk (2003)], inverted stepped pyramidal DRAs [Petosa (2007)], U-shaped DRA excited by elliptical conformal patch [Zhang et al. (2008)], fractal and CPW fed fractal DRA [Dhar et al. (2013)], cup-shaped inverted hemispherical DRA [Mukherjee et al. (2013)], and uniaxial anisotropic rectangular dielectric resonator antennas [Fakhte et al. (2017b)].

(d) Hybrid antennas: The combination of DRs and radiating patch/slot with closer resonant frequencies provides the hybrid approach to enhance the bandwidth of DRAs. Some of the hybrid systems include: combination of circular microstrip patch and ring shaped DR fed by a slot [Perron et al. (2009)], monopole antenna with ring dielectric resonator [Guha et al. (2006a)], combination of CPW inductive slot and rectangular DR [Gao et al. (2006b)], and cylindrical DR with inductive slot [Lin et al. (2009)].

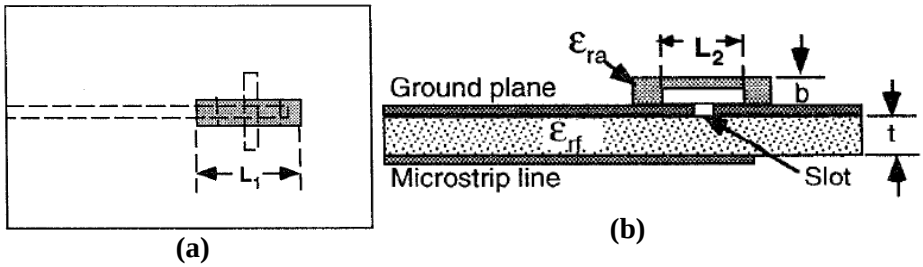

(a) (b)

Configuration of a rectangular DRA (a) top view (b) side view [Ittipiboon et al. (1996)]

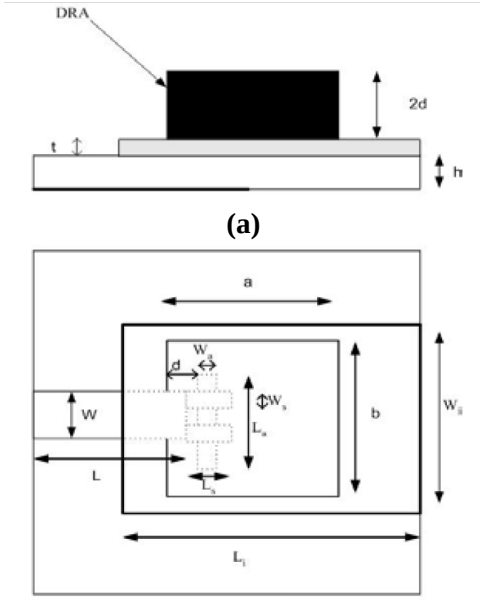

(a) (b)

Configuration of a rectangular DRA (a) side view (b) top view [Coulibaly et al. (2006)]

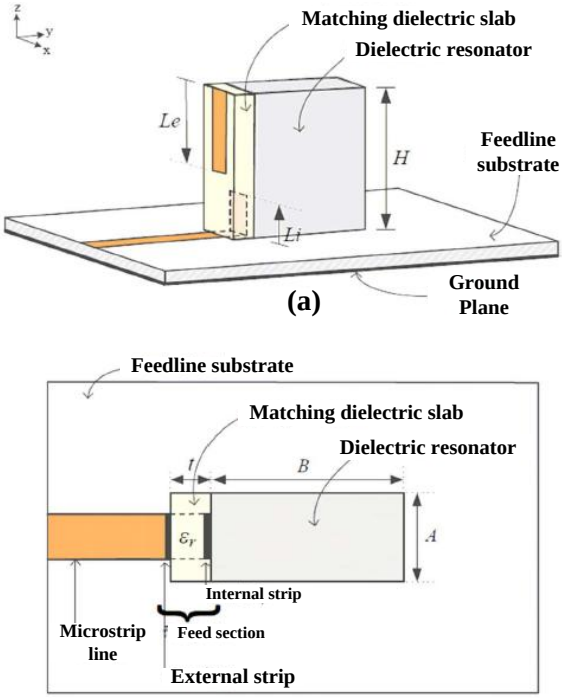

(a) (b)

Configuration of DRA (a) 3D view (b) top view [Rashidian et al. (2012)]

Figure 1.1 Different types of DRA configurations providing improved bandwidth.

Figure 1.1 shows some DRA configurations providing improved bandwidth. Ittipiboon et al. (1996) reported that a wider operational impedance bandwidth of a dielectric resonator antenna can be obtained by lowering its Q-factor. The Q-factor of dielectric ring resonators can be reduced by increasing the ratio of the inner to outer radii, thus lowering the amount of stored energy. It is expected that by removing the centre portion of the DRA, its bandwidth can be increased. Coulibaly et al. (2006) have investigated an

antenna having a dielectric resonator (ε_r = 10.2), an intermediate substrate (ε_r = 2.2) and a microstrip fed slot and got 59% of measured impedance bandwidth. Rashidian et al. (2012) reported a compact wideband multimode dielectric resonator antennas fed with parallel standing strips and obtained over 60% impedance bandwidth with broadside radiation patterns.

1.2.4 Radiation pattern

The radiation pattern represents the radiation properties of the antenna as a function of space coordinates. Generally, radiation properties are checked in the far-field region where the spatial (angular) distribution of the radiated power does not depend on the distance. The radiation pattern typically describes the normalized field (power) values with respect to the maximum value.

For linearly polarized antennas, their performance is usually described with respect to their radiations in the E- and the H-planes. The E-plane is the plane containing the electric-field vector and the direction of maximum radiation, whereas the H-plane is the plane containing the magnetic-field vector and the direction of maximum radiation [Balanis (2005)].

The radiation patterns of the antennas which are commonly encountered are described below:

(a) Isotropic antenna: An ideal, theoretical and lossless antenna which radiates equally in all directions. The radiation pattern of the antenna is used as a reference for expressing the radiation properties of actual antennas.

(b) Directional antenna: An antenna which radiates more efficiently in a particular direction. This is usually valid for an antenna where its maximum directivity is considerably more than that of a half-wave dipole.

(c) Omnidirectional: An antenna which has an essentially non-directional radiation pattern in a given plane and a directional radiation pattern in any orthogonal plane.

A monopole antenna in general provides omni-directional radiation pattern. The DRAs producing monopole like radiation pattern so far include dielectric ring resonators [Ittipiboon et al. (2005); Lapierre et al. (2005); Ong et al. (2002) (2004)], triangular resonators [Gangwar et al. (2017); Kumari et al. (2018b)], half hemispherical [Guha et al. (2006c)], half cylindrical [Rajan et al. (2015)] and cylindrical resonators [Guha et al. (2006b); Chaudhary et al. (2012)]. To achieve monopole like radiation pattern, different multi-element DRAs have been widely investigated and reported in the literature. Four element cylindrical DRA (CDRA) along with additional central composite probe [Guha et al. (2006b)], multi-layer multi-permittivity (MLMP) CDRA with MLMP central probe [Chaudhary et al. (2012)], 4-element triangular DRA (TDRA) [Gangwar et al. (2017)], and 4-element composite TDRA [Kumari et al. (2018b)] have been investigated previously for the generation of monopole like radiation pattern (Figure 1.2). However, these DRAs show much complexity in their design and fabrication, which is not desirable at the medium or pilot scale production due to high manufacturing cost and time involved. Therefore, in the present study, more emphasis is given on the design of DRAs with simpler structure, for obtaining monopole like radiation pattern.

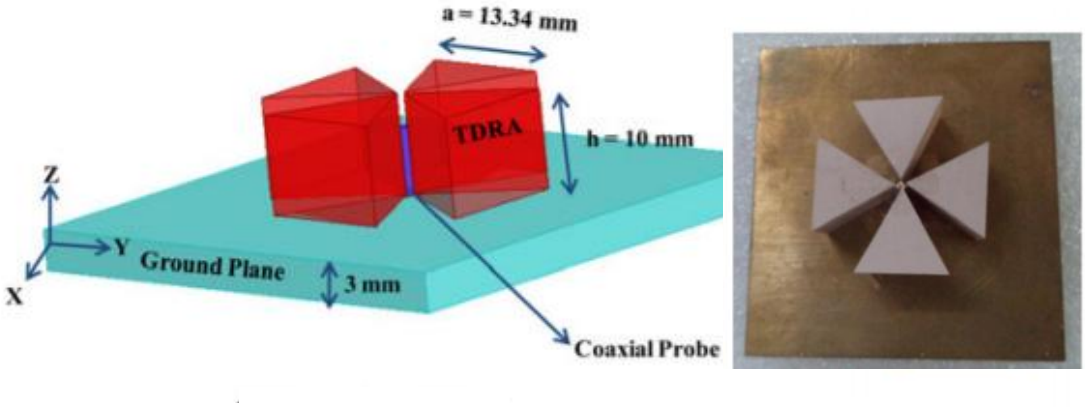

(a) (b)

Four-element triangular DRA (a) 3D view, (b) Fabricated antenna Prototype [Gangwar et al.(2017)]

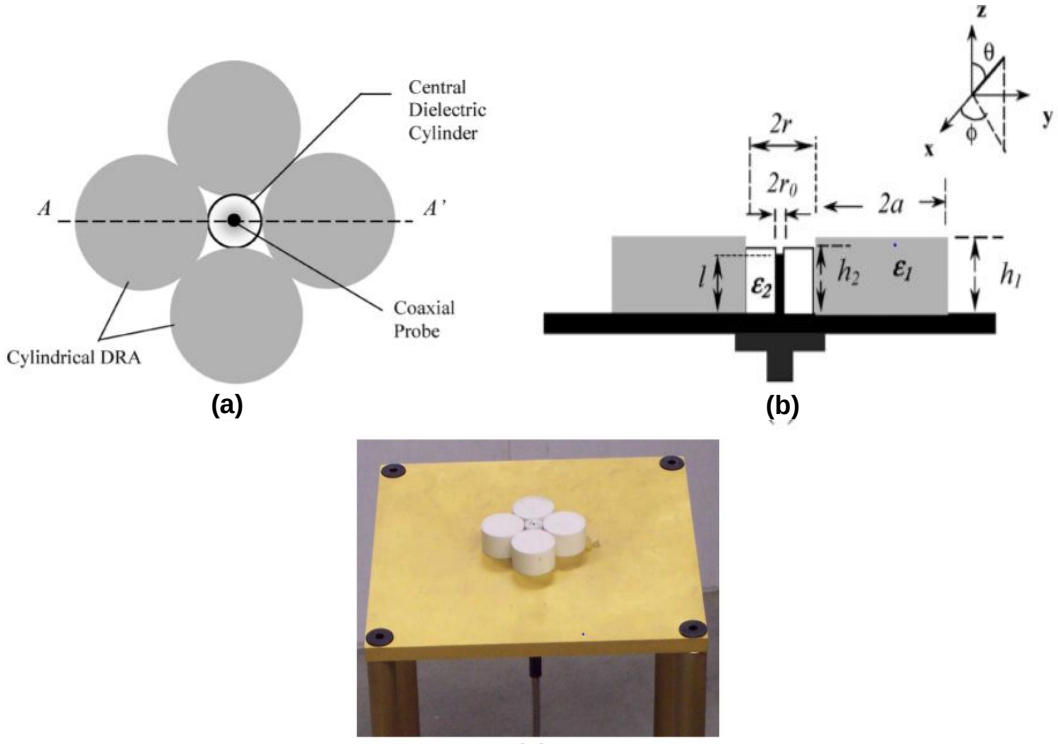

(a) (b)

(c)

Four-element cylindrical DRA (a) Top view, (b) cross-sectional view at AA' plane and (c) Fabricated antenna prototype [Guha et al. (2006b)]

Figure 1.2 Different complex multi-element DRAs generating monopole like radiation pattern.

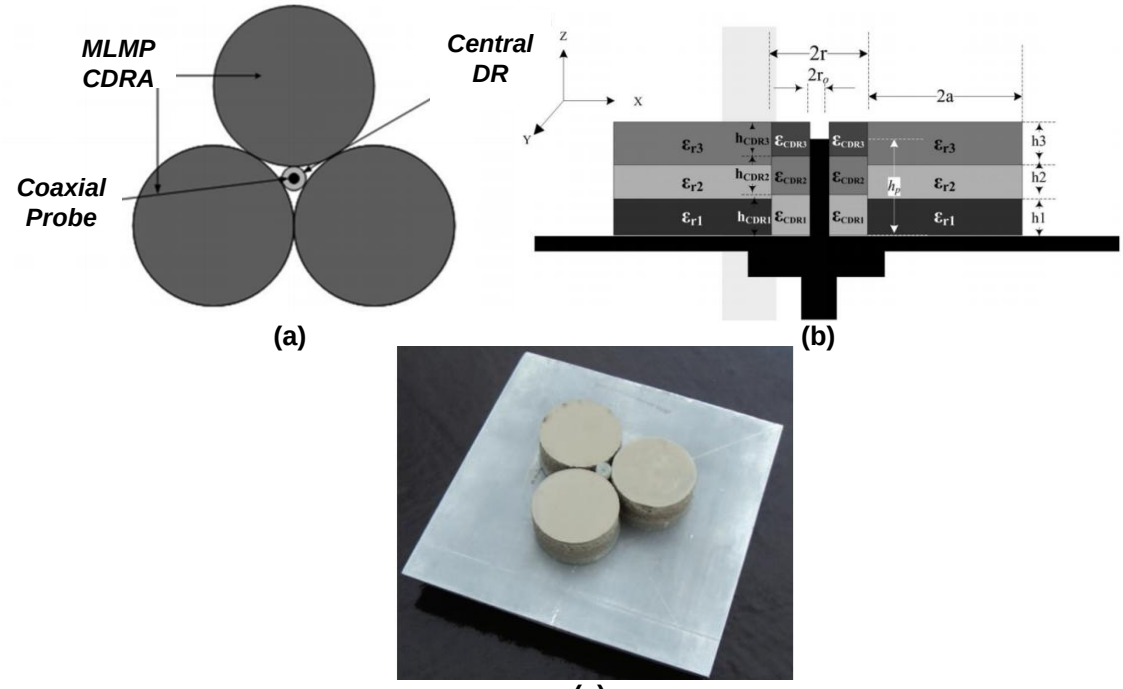

Three-element MLMP CDRA with MLMP central CDR fed by coaxial probe (a)Top View, (b) Cross-sectional view and (c) Fabricated antenna prototype [Chaudhary et al. (2012)]

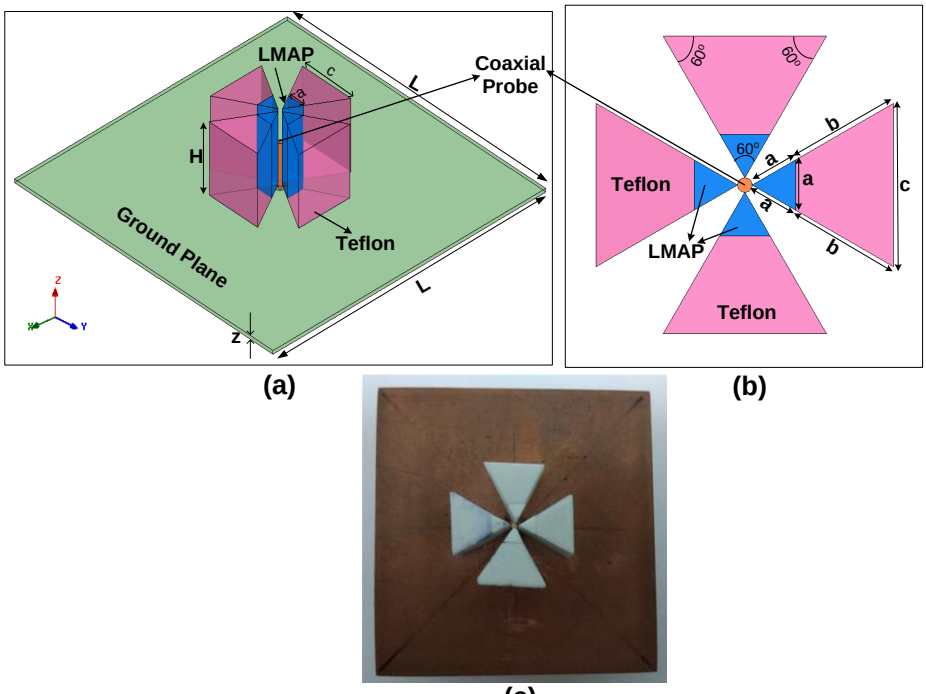

Geometry of proposed composite TDRA (a) 3D view, (b) Top view and (c)Fabricated antenna prototype [Kumari et al. (2018b)]

Figure 1.2 contd. Different complex multi-element DRAs generating monopole like radiation pattern.

1.2.5 Gain

The directivity, D, is defined as the ratio of the radiation intensity (U) in a given direction from an antenna over that of an isotropic source (U_o). In addition, since the radiation intensity for an isotropic source is known, the directivity can be expressed as [Balanis (2005)]

$$D = \frac{U}{U_o} = \frac{4\pi U}{P_{rad}} \tag{1.9}$$

where U is the radiation intensity of the antenna, U_o is the radiation intensity of the isotropic source and P_{rad} is the radiated power of the isotropic source.

If the value is not specified, the directivity of an antenna implies its maximum value, D_o. This is given by [Balanis (2005)]

$$D_o = \frac{U_{max}}{U_o} = \frac{U_{max}}{U_o} = \frac{4\pi U_{max}}{P_{rad}} \tag{1.10}$$

Although the gain, G, of an antenna is related to the directivity of the antenna, it takes into account the radiation efficiency of the antenna as well. The relation is given by [Balanis (2005)]

$$G = E_{rad}D \tag{1.11}$$

where E_{rad} is the radiation efficiency of the antenna and D is the directivity of the antenna. Similar to eq. (1.11), the maximum gain of an antenna, G_o, is related to the maximum directivity, D_o, as given by [Balanis (2005)]

$$G_o = E_{rad}D_o \tag{1.12}$$

1.2.6 Gain enhancement techniques for DRAs

Gain is one of the most important parameters of an antenna. Various methods are available to enhance the gain of DRAs. Arraying of DRAs is one of the basic approaches to increase the gain of the antenna, in which, gain is increased by increasing the number of DR elements. The disadvantage of this approach is that it requires significant amount

of DR material. Engraving notches on two opposite side walls of DR increases the radiation from side walls as compared to its top wall for its fundamental mode resulting in enhanced gain [Fakhte et al. (2017a)]. Placement of different designs of substrates (mushroom like, strip corrugated and coaxially corrugated EBG substrates [Llombart et al. (2005)], circularly periodic EBG substrate [Coulibaly et al. (2007)] suppress the surface wave propagation in all radial directions resulting in the increase of antenna gain. Other efficient approaches to enhance the gain of DRAs include generation of higher order modes (by single or composite excitation), stacking of parasitic DRA on the top of driven DRA with a space [Petosa et al. (2009)], placement of pyramidal horn surrounding the DRA [Yarge et al. (2009)], using uniaxial anistropic (single crystal) dielectric materials in fundamental mode [Fakhte et al. (2017b)], optimization of place of excitation and layer thickness [Yarge et al. (2009)], placement of superstrate or metamaterial at particular height above the DRA [Antar (2008)], positioning circularly polarized DRA in circular cavity [Carrie (1996a) (1996b)], and using composite dielectric substrate [Chattopadhyay et al. (2009)].

1.3 Excitation of DRAs

The selection of types of excitation and their location, both play significant role on the resonant frequency, input impedance bandwidth and radiation characteristics of the DRA. General feeding methods for excitation of DRAs, such as co-axial probe feed, microstrip line feed, aperture-coupled feed, co-planar waveguide feed and dielectric image guide feed are described below .

1.3.1 Coaxial probe feed

In probe excitation technique, strong coupling can be achieved by locating the probe in high E-field region of DRA. Therefore, the probe is either inserted into the dielectric resonator so that its outer surface touches the resonator everywhere or kept touching the

outer surface of dielectric resonator or it is located adjacent to resonator. The height, depth of penetration and position of the probe are optimized to achieve maximum impedance bandwidth. Different types of modes can be generated by changing the location of the probe. The drilling of hole in the substrate and / or dielectric resonator is required for insertion of the probe. The advantage of probe feed is that, it can be coupled directly with 50 Ω system without using matching network. This type of feed is generally used for relatively lower frequency applications.

1.3.2 Microstrip line feed

In this coupling mechanism, the dielectric resonator is placed just above or in proximity with the open circuited end of the microstrip line. The amount of impedance matching depends on the lateral position of dielectric resonator with respect to microstrip feed line. Dielectric constant of DRA affects significantly the degree of coupling. Strong coupling can be achieved for dielectric resonator having dielectric constant value greater than 20. This method shares the merits of using a coaxial probe, but avoids the need for drilling a hole into the dielectric. This type of feed is mainly used in the DRA integrated with MMICs without the need for a coupling slot [Luk et al. (1999)].

1.3.3 Aperture-coupled feed

In the aperture-coupled feed, the feedline structure is no longer in contact with the dielectric resonator. The resonator is kept just above the slot provided in the ground plane. The slot can be fed by a microstrip coating or a waveguide. There is flexibility in the design of the feedline and the DRA in aperture-coupled feed technique of excitation. The aperture behaves as a magnetic current parallel to the length of the slot and excites the magnetic field in the DRA. The radiation from the microstrip feed significantly decreases and this improves the quality of polarization as well. This coupling mechanism has the following advantages: i) DRA can be easily integrated with the feed structure, ii)

Drilling of hole is also not required as in case of coaxial probe feed [Sebastian et al. (2017)], and iii) Radiating aperture is isolated from the spurious radiation from the feed. A major drawback of the technique is that it cannot be used for lower frequency (at and below L-band) applications because of large size of slot required.

1.3.4 Coplanar waveguide feed

This feed is uni-planar and thus provides good integration of the DRA with other active circuit components on the same side of substrate without the need of vias. This feeding technique is less dispersive in nature and provides low conductor losses and low radiation leakage. It is suited for millimeter wave applications because of reduced surface wave excitation in electrically thick substrates as compared to microstrip feed [Sebastian et al. (2017)].

1.3.5 Dielectric image guide coupling feed

Unlike microstrip line, the dielectric waveguide does not suffer from conductor and surface wave losses at millimeter-wave frequencies. In the DRA, particularly with low dielectric constant, the amount of coupling using microstrip line is quite low. To increase the coupling, a low loss dielectric image guide is used as feed for linear DRA array [Petosa (2007)].

1.4 Modes of Excitation

Simple shaped DRAs: rectangular, cylindrical and hemispherical DRAs with and without modification are commonly used for signals radiated at gigahertz frequencies. The desirable features of DRAs include high gain, wide impedance bandwidth, enhanced efficiency and application based radiation patterns. Excitation of particular mode/modes is required for the desired performance of DRAs. This is achieved through proper selection of feed type (microstrip line feed, probe feed, aperture coupling etc.) and its location. To excite particular mode/modes, knowledge of corresponding electric and

magnetic field configurations is essential. The modes generally excited within different shapes of DRAs which give broadside radiation patterns over wide frequency range similar to an electric or magnetic dipole are listed in Table1.1.

Table 1.1 Modes of excitation in different shapes of DRA

S.No.	DRA shape	Excited Mode
1.	Hemispherical/ conical shaped dielectric ring resonator [Guha et al. (2012)]	• TE_{111}mode (Radiates like short horizontal magnetic dipole). • TM_{101} (Radiates like short electric monopole) – generally probe feed is used for excitation
2.	Half-Hemispherical DRA[Guha et al.(2006c)]	• $HEM_{11\delta}$ like mode • TM_{101} like mode
3.	Pawn-shaped DRA[Guha et al. (2009)]	• TM_{01} like mode
4.	Cylindrical DRA [Petosa (2007)]	• $TM_{01\delta}$ (Radiates like short electric monopole) • $TE_{01\delta}$ (Radiates like short magnetic monopole) • $HE_{11\delta}$ (Radiates like short horizontal magnetic dipole) • $HEM_{11\delta}$ (Generally excited using probe feed) • $HEM_{12\delta}$ (Higher order mode generally excited using aperture coupling) • $HEM_{21\delta}$ (Higher order mode) • HEM_{111} (Higher order mode generally excited using aperture coupling) • HEM_{113} (Higher order mode generally excited using aperture coupling)
5.	Dielectric Ring Resonator	• TM_{01} (Monopole like radiation pattern)
6.	Cylindrical Antenna [Guha et al.(2006b)]	• $HEM_{11\delta}$ like mode
7.	Rectangular DRA [Luk and Leung (2003)]	• $TE^{x}/TE^{y}/TE^{z}$ (Radiation like short magnetic dipole in x, y and z directions respectively) • $TE^{x}_{\delta 11}/TE^{y}_{1\delta 1}/TE^{z}_{11\delta}$ (Lower order mode) • $TE^{x}_{\delta 31}/TE^{y}_{\delta 13}/TE^{z}_{\delta 21}$ (Higher order mode)

Various modes providing different radiation characteristics can be excited through the exploitation of different feeding techniques. The most widely investigated shape of DRA

is the cylindrical one. Different types of radiation patterns according to category of application can be generated using the cylindrical DRA (CDRA) by exciting a single (pure) mode or hybrid mode. $TE_{01\delta}$ and $TM_{01\delta}$ modes, which are lower order modes get excited in the CDRA. $TE_{01\delta}$ mode generated in CDRA radiates like a magnetic dipole and hence, it is potentially used for communication between satellites and different locations of earth, whereas $TM_{01\delta}$ mode generated in CDRA radiates like electric monopole and finds application in areas where monopole pattern is desired. Some higher order hybrid modes i.e $HE_{11\delta}$, $HE_{21\delta}$, $EH_{11\delta}$ and $EH_{21\delta}$ also excited in CDRA radiate like magnetic dipole, magnetic quadrupole, electric dipole and electric quadrupole respectively [Mongia et al. (1994)]. When the aperture-coupled feed is used for the excitation of CDRA, hybrid electro-magnetic (HEM) mode is generated and broadside radiation pattern is achieved [Guha et al. (2015)]. Van Bladel asymptotic theory says that non-confined mode is present in non-uniform shape of DRA. The expected dominant mode contributing for radiation is like a magnetic dipole resulting in greater probability of the presence of $TE_{01\delta}$ and $HE_{01\delta}$ modes [Bladel et al. (1975a) (1975b)].

1.5 Dielectric Materials and their Properties

1.5.1 Parameters of ceramic dielectric materials affecting the performance of DRAs

Some important material constraints of dielectric resonator are described here which affect the performance of DRAs.

(a) Dielectric constant/relative permittivity: The dielectric constant (ε_r) values should be in the range 5 - 30 for efficient antenna performance. In general, it should be noted that decrease in permittivity of the resonating material of the DRA can improve the radiation properties over a wider operating frequency range. Hence, low dielectric constant and low loss materials are preferred for wideband applications. The wavelength

of the electromagnetic wave traversing through the dielectric material is inversely proportional to the square root of the material dielectric constant or relative permittivity. So, the high dielectric constant resonator can effectively reduce the size of the DRA for microwave frequency applications. The wavelength in the dielectric material (λ_d) can be calculated as [Sebastian et al. (2017)]:

$$\lambda_d = \frac{\lambda_o}{\sqrt{\varepsilon_r}} \tag{1.13}$$

where λ_o is the wavelength in air or vacuum and ε_r is the dielectric constant of the material.

High dielectric constant materials (80-100) can be used for low profile applications when bandwidth is not the main concern. For cylindrical and rectangular DRAs, the bandwidths fall in the ranges of 35 - 40 %, and 20 - 40% respectively. For typical antenna application, it is recommended to use a low loss material with dielectric constant in the range 8-20 [Sebastian et al. (2017)].

(b) Effective dielectric constant/relative permittivity:

$$\varepsilon_{eff} = \frac{H_{eff}}{\frac{h}{\varepsilon_r}+\frac{t}{\varepsilon_i}+\frac{s}{\varepsilon_s}} \tag{1.14}$$

where H_{eff}= h+t+s, 'h' is DRA height, 't' is insert thickness, 's' is substrate thickness, 'ε_r' is dielectric constant of DRA, 'ε_i' is dielectric constant of insert, and 'ε_s' is dielectric constant of substrate. Slots in DRA reduce the effective permittivity of DRA which provides wider bandwidth [Petosa (2007)].

(c) Dissipation factor (loss tangent/dielectric loss): Dissipation factor = ε"/ε', where ε' is the real part of permittivity and ε" is the imaginary part of permittivity. Low dielectric loss (< 0.002) is generally preferred for the DRA.

(d) Temperature coefficient of resonant frequency (τ_f): The temperature coefficient of resonant frequency decides the thermal stability of the dielectric resonator.

The DRAs should have near zero temperature coefficient of resonant frequency for radr and wireless communication applications.

(e) Sample size/thickness: Size of DRA is proportional to $\lambda_o/\sqrt{\varepsilon_r}$, where λ_o is free space wavelength at the resonant frequency and ε_r is the dielectric constant of material. Therefore, size of DRA depends upon resonant frequency and dielectric constant of the material.

1.5.2 Parameters affecting the dielectric constant of the resonator

Some important material parameters, which affect the dielectric constant of the resonator are described below.

(a) Refractive index (η): The dielectric constant of dielectric materials measured at microwave frequencies is directly proportional to the square of the refractive index η of these materials measured at optical frequencies. The relation, $\varepsilon_r = \eta^2$ is accurate only when ε_r and η are measured under same conditions. This has been found true in case of diamond (ε_r= 5.68, η^2 = 5.85) and germanium (ε_r= 16, η^2= 16.73) [Moulson and Herbert (2003)]. But the phenomenon is not always true for all types of dielectric materials. Since the dielectric constant is frequency dependent and the possibility of getting same dielectric constant at microwave frequencies as per the aforesaid relation in terms of refractive index is very low. In case of diamond and germanium, the same polarisation processes are getting generated at optical and microwave frequencies. On the other hand, for other materials, the dipolar polarisation processes excited at lower frequencies do not generally happen at higher optical frequencies. The dipolar and ionic polarizations mainly contribute to the permittivity at microwave frequencies.

(b) Internal structure of materials: Dielectric constant (ε_r) is directly proportional to polarization (creation of resultant positive and negative charges) whose strength is only

decided by crystal structure of materials. Homogeneous materials give good and uniform permittivity values throughout the volume.

(c) Temperature: Increasing the temperature results in decrease in value of dielectric constant for high permittivity materials because dipolar (orientational) polarization decreases, and increase in value of dielectric constant of low permittivity materials due to generation of more charges and ions which results in increase of orientational polarization.

(d) Hysteresis: The polarization-electric field hysteresis, is a defining property of ferroelectric materials. In ferroelectric memories the information is stored as positive or negative remanent polarization state. The hysteresis behaviour can be analysed by the relation given below

$$D = \varepsilon_o(1+ \chi_e)E = \varepsilon_o\varepsilon_r E \quad (1.15)$$

where D is dielectric displacement, ε_o is dielectric constant of vacuum, ε_r is dielectric constant of material, χ_e is dielectric susceptibility and E is electric field strength. Dielectric constant (ε_r) depends on electric field strength for nonlinear materials.

(e) Density: Density is directly proportional to dielectric constant (ε_r) of the material.

(f) Frequency range of operation (bandwidth): Frequency range of operation depends upon the dielectric constant (ε_r) and dimensions of the material.

1.5.3 Effect of interaction of radio-frequency field with dielectric materials

In dielectric materials, all charges are attached to specific atoms/molecules. These charges are called bound charges. By applying external electric field, positive and negative charges of neutral body are displaced slightly from their respective positions and form induced dipole moments whose directions align in the direction of applied external electric field. These dipoles produce their own electric field. The resultant electric field i.e. the combination of applied field and the dipole field is called the internal field.

Particles having permanent dipole moment experience electrical torque in the presence of external applied field. Interaction of EM wave (composed of photons) with materials can be explained through macroscopic Maxwell's equations together with constitutive relations and boundary conditions. EM wave consists of packets of photons. When EM wave of appropriate frequency interacts with atoms of a material, photonic energy is either absorbed or emitted by the atoms. When an atom emits photons, energy of the atom is decreased and energy of EM wave is increased. When the high energy photons of EM wave collide with atoms/molecules of the material, these photons give their energy to them due to which the atoms/molecules move through the material and deposit their kinetic energy into surrounding matter.

Dielectric and magnetic polarizations occur due to permanent or induced dipole moments caused by applied field and spin moments. When applied electric field interacts with dipole moment of molecules or atoms, potential energy of molecules or atoms is converted into kinetic energy due to promotion of rotational and atomic transitions. This effect is known as Stark Effect. Rotational and atomic transitions depend upon frequency and strength of applied field. The effect which describes the interaction of magnetic field with dipole moment of molecules and atoms is known as Zeeman Effect.

(a) Material response to applied EM-field: When EM-field is suddenly applied to a dielectric material, following fields appear that cause system to acquire non-equilibrium state for certain period of time.

1. Macroscopic electric field (E): E= (E_a-E_{dp}) or (E_a-p/3ε), where Ea is the applied electric field, E_{dp} is the depolarization field, p (= αE_l) is the induced electric dipole moment, α is the polarizability, E_l is local electric field strength, and ε is the absolute permittivity.

2. Depolarization field (E_{dp}): This field is generated due to particle back reaction field from charge, spin and current rearrangements. This field opposes the applied electric field.

*3. Local field (E_l):*This field is generated due to average EM field at a particle site because of both the applied field and field created by other sources, such as dipoles, currents, charges and spin.

*4. Microscopic field (E_{micro}):*It is generated due to particle interacting with the field generated by discrete charges.

5. Applied electric field (E_a): It is generated due to external power sources.

When EM-field (varying with time) is applied to the material, atoms, molecules, free charges, and induced / permanent dipoles and defects change their positions/ orientations according to varying EM-field but with some time lag, known as relaxation time. The dynamic readjustment of atoms and molecules after interaction with EM-field is called relaxation. The time lag may be due to screening, friction, inertia and coupling. Various phenomena occur during the relaxation: i.e. heat conversion, photon-phonon and lattice-phonon interactions, defect diffusion and/ or higher multi-pole interactions. Response of material at the time of interaction with EM-field depends strongly on the material composition and lattice structure.

The crystal structure, permanent dipoles, mobility of free charges and defects contribute to the dielectric properties of material. The solids, which do not appreciably rotate or polarize due to applied EM-field have low dielectric constant values, whereas the solids which rotate or polarize appreciably according to applied EM-field have high dielectric constant values. At RF/microwave frequencies, high and low loss materials respond differently. At RF/microwave frequencies, dipolar, ionic and electronic polarizations

occur. Therefore, vector dipole moment $\mu_d = (\alpha_{dip} + \alpha_{ion} + \alpha_{el})E_l$, where $\alpha_{dip} = |\mu_e|^2/3K_BT$, $\alpha_{ion} = e^2/Yd_o$, $\alpha_{el} = 4\pi\varepsilon R^3/3$. Here μ_e is permanent dipole moment, K_B is Boltzman constant, T is absolute temperature, R is radius of ions, d_o is equilibrium separation of ions and Y is young's modulus [Jarvis and Kim (2012)].

(b) Modified Clausius- Mossotti relation: The equation

$$(\varepsilon_r-1)/(\varepsilon_r+2) = (N/3\varepsilon)[\alpha+|\mu_e|^2/3K_BT] \quad (1.16)$$

where N is density of dipoles and ε is absolute permittivity, provides the relation between permittivity and polarizability for all types of materials (solids, liquids and gases). The equation reveals the information that when EM-field interacts with the material, various phenomena occur at macroscopic and microscopic levels within the material causing different types of polarizations which affect the permittivity of the material.

(c) Losses during interaction of RF/microwave field with material: Dielectric losses occur within the polar materials because of friction caused by rotation, free charge movement and out of phase dipole coupling. Losses occur in non-polar materials due to interaction with neighboring permanent and induced dipoles, intrinsic phonon- photon interaction in presence of EM-field and losses caused by grain morphology, defects and dislocations. In high purity crystals, anharmonic coupling with electric field and presence of defects allow photon- phonon interaction that introduces losses. Centro-symmetric dielectric crystals experience lower losses than non-centro symmetric crystals.

1.5.4 Laboratory synthesized and commercially available dielectric materials

Electrical insulator materials can be termed as dielectric materials. They can be polarized by an applied electric field. When a dielectric material is placed in an electric field, the positive and negative electric charges slightly shift from their average equilibrium positions causing polarization. This creates an internal electric field which reduces the

overall field within the dielectric and electrical energy stored within the material reduces up to maximum, and radiation can occur from the floating end where such a material is placed on the ground plane. Dielectric ceramics are potential ceramic materials, which are used for the design of DRAs.

Ceramic dielectrics are extensively used in radar and wireless communication systems as well as electronic devices. For practical applications, these materials are usually prepared by conventional ceramic fabrication routes such as, solid state route, liquid phase sintering or chemical processing. The dielectric material properties depend considerably on the chemical composition, porosity, crystal structure and imperfections in the crystal lattice. The fabrication condition also influences the material properties, e.g. calcination conditions influence the structure, secondary phase formation and dielectric characteristics. The secondary phase plays an important role in controlling the density, microstructure, grain growth and RF/microwave dielectric properties of the ceramic resonator materials. The purity of raw material plays an important role on the sintering conditions and dielectric properties. Large number of laboratory synthesized materials are reported by Sebastian et al. (2008) (2017). Some common commercially available dielectric materials are listed in Table 1.2.

Table 1.2 Commercially available dielectric materials for DRA applications

S.No.	Dielectric Material	Dielectric Constant (ε_r)	Tangent Loss (tanδ)
1	PTFE (Polytetrafluoroethylene or Teflon)	2.1	0.0002 @ 3 GHz
2	FR-4	4.4	0.008 @ 3 GHz
3	RT duroid	2.3	0.0012
4	Alumina (Al_2O_3)	10.2	0.0002 @ 1 GHz
5	Wood	1.2-2.1	0.03 @ 3 GHz
6	Soil	2.44	0.0011 @ 3 GHz
7	Neoprene Rubber	4	0.034 @ 3 GHz
8	Silicon	11.7-12.9	0.005 @ 1 GHz
9	GaAs	13.1	0.0016 @ 10 GHz

1.6 Recent Developments Pertaining to DRAs

Now-a-days, DRAs are drawing great attention for the radar and wireless communication due to their attractive advantages, such as large bandwidth, ease of excitation, high radiation efficiency, low phase noise, flexible feed arrangement, ease of integration with other active or passive microwave integrated circuit components, easily controlled characteristics and wide range of material dielectric constants. DRAs can be excited by different feeding techniques: coaxial or probe, microstrip line, slot, coplanar waveguide and dielectric image guide. The conventional shapes of DRAs: rectangular, cylindrical, hemispherical, and ring provide a typical bandwidth of around 10%, which may not be adequate for wideband applications. Bandwidth enhancement of a DRA, especially with a low profile design is a demanding task for the researchers. Different approaches are used to enhance the bandwidth of DRAs [Shum and Luk (1985), Rao et al. (2006)]. Multi-element stacking is one of the approaches to enhance the bandwidth but overall antenna volume is increased in this approach. Another approach includes the merging of a hybrid radiating mode with the DRA mode. Such merger of modes occurs in dielectric resonator on patch configuration [Esselle and Bird (2005)] and coplanar waveguide inductive slot embedded as a hybrid radiator along with the DRA [Gao et al. (2006a)]. By merging resonances of rectangular (RDRA) and probe feed, wideband hybrid design can be obtained [Zou and Pan (2015)]. To achieve wideband impedance match, some special feeding mechanisms viz. L-shaped probe feed in cylindrical DRA [Kishk et al. (2006)] and tall microstrip transmission line (TML) [Rashidian et al. (2014)] are also used. The TML-DRA configuration can offer bandwidth up to a maximum of 25% with more complex construction. Several DRA geometries, such as H-shaped [Liang and Denidni (2008)], T-shaped [Gao et al. (2012)], dumb-bell shaped DRAs [Chaudhary et al. (2014)] were analyzed for wideband applications. Material selection for the DRA also plays an

important role in deciding the final antenna performance. For the DRA performance to be effective, both the aspects i.e. DRA configuration and the DRA material selection need to be considered. It is possible to get good DRA performance using proper material with simple configuration instead of going for complex configuration with improper material selection. Thus, state-of-the art of various types of dielectric resonator materials is also discussed in the present article. The performance of recently designed DRAs with commercially available and synthesized ceramic materials is described in Table 1.3.

Table 1.3 Recently designed DRAs with commercially available and synthesized ceramic materials.

S.No	Dielectric Material and Reference	DRA Shapes	Bandwidth, (%)	Excitation Mechanism	Mode	Application
1.	Al_2O_3 (ε_r=9.8) Sharma et al.(2016d)	Cylindrical DRA	9.13, 11.9,30.2%	Ring-shaped patch along with an inverted L-strip (microstrip line)	$HE_{11\delta}$, $HE_{12\delta}$	WLAN (2.4 GHz) and WiMAX (2.5/3.5 GHz)
2.	Al_2O_3 Das et al. (2017)	Cylindrical DRA	11.5%	Dual feed (Aperture coupling and CPW)	$HE^{x}_{11\delta}$ and $HE^{y}_{11\delta}$	MIMO applications
3.	Al_2O_3 Gupta et al. (2016)	Dual segment RDRA	23.1%	Conformal strip (microstrip line)	$TE_{1\delta1}$	Radar and satellite application (S-band)
4.	Al_2O_3 Gangwar et al. (2016)	Hybrid cylindrical DRA	13.3, 24.1, 7.9%	Annular ring shaped patch along with T-shaped printed line (Microstrip line)	$HE_{11\delta}$, $HE_{12\delta}$	WLAN(2.4/5.8 GHz) and WiMAX (2.5/3.5/5.5 GHz)
5.	Al_2O_3 Sharma et al. (2016c)	Stacked CDRA	100.9%	Annular shaped (Microstrip line)	$TE_{01\delta}$, $TM_{01\delta}$	Ultra wide band antenna application for high data rate
6.	Al_2O_3 Sharma et al. (2017a)	CDRA	18.0,19.8%	Modified circular shaped aperture	$HE_{11\delta}$, $HE_{12\delta}$-like $HE_{12\delta}$	WLAN(2.4/5.2/5.8 GHz) and WiMAX (2.5/5.5 GHz)
7.	Al_2O_3 Sharma et al. (2017b)	Composite CDRA	21.4, 25.3, 10.3%	Modified annular ring printed line with U-shaped printed Microstrip line	$HEM_{11\delta}$, $HEM_{12\delta}$	WLAN and WiMAX applications

8.	Al_2O_3 Gupta et al. (2013)	Three element dual segment triangular DRA	22.9%	Co-axial probe feed	TM_{10-1}	X-Band applications
9.	Al_2O_3 Gupta et al. (2017)	4-Element dual segment RDRA array	13.7 %	Copper strip excitation (connected to microstrip line)	$TE^{y}_{1\delta1}$	Radar and satellite application
10.	Al_2O_3 Rajan et al. (2015)	Half split cylindrical DRA	51.2%	Probe feed	$TM_{01\delta}$	WLAN and WiMAX
11.	Al_2O_3 Sahu et al. (2017)	CDRA	19.1, 38.0, 18.5%	Modified annular ring patch feed	$HEM_{11\delta}$, $HE_{12\delta}$	WLAN / WiMAX
12.	Al_2O_3 Sharma et al. (2015)	Two segment CDRA	8.3,17.1, 39.9%	Microstrip line along with two ring patch	$HE_{11\delta}$, $TM_{01\delta}$	WLAN/ WiMAX
13.	Al_2O_3 Sharma et al. (2016a)	Hybrid MIMO CDRA	6.1, 26.4, 35.7%	Two symmetric folded microstrip line feed	$HEM_{11\delta}$	LTE2500/ WLAN/ WiMAX
14.	Al_2O_3 Sharma et al. (2016b)	CDRA	18.8, 2.6, 7.5 %	Composite feed (combination of vertical strip and psi-shaped (ψ) microstrip line)	$HEM_{11\delta}$, $TM_{01\delta}$, and $HEM_{12\delta}$	WiMAX (2.5 GHz) and vehicular applications
15.	Al_2O_3 Kumar and Chaudhary (2016)	Cubic DRA	BW_{im}=35.3% BW_{AR}=20.6%	Question-mark-shaped microstrip feed	$TE_{11\delta}$	WiMAX (3.3–3.7 GHz)
16.	Al_2O_3 Kumari and Gangwar (2017)	CDRA	BW_{im} = 40% BW_{AR} = 9%	Dual conformal strips with modified Wilkinson power divider	-	Bluetooth and Wi-Fi
17.	Al_2O_3 Abdulmajid et al. (2018)	Rectangular DRA	2.3,9.5%	Microstrip line with cross slot	TE_{117}, TE_{119}, $TE_{11,11}$, $TE_{11,13}$	mm-wave and terahertz higher frequency bands
18.	Al_2O_3 Yang and Pan (2018)	Square DRA	49.5%	Microstrip-coupled cross-slot	TE_{111}	Radio frequency identification (RFID) system, Global positioning system and satellite communication/ navigation system

19.	Al_2O_3 Chowdhary and Chaudhary (2018)	Modified cylindrical shaped dielectric resonator antenna	51.2%	Probe feed	-	Modern wireless communication system
20.	Al_2O_3 Ahmad and Barth (2018)	Spherical	9%	Microstrip resonator and microstrip feed line	TE_{113}	High data-rate communication and sensing
21.	$SrLa_2Mg_2W_2O_{12}$ (ε_r = 22) Sahu et al. (2013)	Dual segment CDRA	16.9%	Probe feed	-	X-Band applications
22.	$SrLa_2Mg_2W_2O_{12}$ (ε_r = 22) Sahu et al. (2013)	Dual segment CDRA with meta-material	25.3 %	Probe feed	-	Radio navigation services, civil and military radar.
23.	Emerson & Cuming Eccostock HIK material (ε_r = 20) Rana and Parui (2015)	CDRA array	2.9%	Non-resonant microstrip patch feed	$HEM_{12\delta}$	Electrically steered array applications
24.	$Nd(Mg_{0.43}Ca_{0.07}Sn_{0.5})O_3$ (εr = 19.51) Chen et al. (2013)	CDRA	12.5,14.2%	Microstrip line feed with rectangular slot	-	Industrial, Scientific medical (ISM), High performance radio local area network (HIPERLAN), Unlicensed national information infrastructure(UNII) bands.
25.	Zirconium Tin Titanate (ε_r = 38) Malekabadi et al. (2008)	Cylindrical DR which is chopped normal to its x axis diameter or rectangular truncation in one side of resonator.	BW_{im}=22.2% BW_{AR}=16.4%	Probe feed	-	-
26.	Li_2O-1.94MgO-0.02Al_2O_3-P_2O_5 (LMAP) (ε_r = 6.2) Kumari et al. (2018b)	Composite triangular DRA	66.1%	Probe feed	TM^z_{101}	broadcast base-stations, radar, and satellite communications
27.	K9 glass (ε_r = 6.85) + liquid ethyl acetate (ε_r = 7.1) Chen and Wong (2017)	CDRA	35.5%	Coaxial probe feed	$HEM_{11\delta}$ and $TM_{01\delta}$	Pattern reconfigurable design without p-i-n diode, suitable for systems which require static changes
28.	10 wt% PBBS Glass-added Barium Strontium Titanate (ε_r = 27) Kumari et al. (2018a)	Dual segment CDRA	11.7%	Aperture coupled feed	-	Radar and radio navigation, military satellite communication

29.	$Zn_{0.7}Mg_{0.3}TiO_3$ (ε_r =15.7) Gangwar et al. (2011)	Cylindrical dielectric resonator antennas	2.11%	Coaxial probe feed	$HEM_{11\delta}$	Wireless communication and radar
30.	ε_r =2.2 Gupta and Gangwar (2015)	Triangular DRA	13.5%, 8.9%	Conformal strip connected to microstrip line	$TM_{10\delta}$, $TM_{30\delta}$	-
31.	ε_r =12 Gangwar et al. (2017)	Four element triangular DRA	37.61%	Co-axial probe feed	$TM_{10\text{-}1}$	-
32.	ε_r =12 Zhang and Wn (2018)	Rectangular cylindrical dielectric resonator and a metallic semi-loop	11.4%	Modified microstrip line feed	-	Massive-MIMO array antennas
33.	ε_r =10.2, ε_r =2.2 Sun and Leung (2018)	Cylindrical DRA array	11.5%	Aperture – Coupled Feed	$HEM_{11\delta}$	Antenna-in-package design
34.	ε_r =38 Tang et al. (2018)	Four-leaf-clover-shaped	9.2%	Probe feed with T shape strip	TE111	Front-end in wireless communication

1.7 Perovskite Ceramics

Perovskite is a naturally occurring mineral with composition $CaTiO_3$. Oxides having the general formula ABO_3 similar to naturally occurring mineral $CaTiO_3$, are known as 'Perovskite Oxides'. An ideal perovskite structure has a cubic unit cell where *A* cation occupies the corner positions, *B* cation occupies the body centre position and oxygen anions occupy the face centered positions of a cubic unit cell (Figure 1.3). Cubic structure often distorted to tetragonal, rhombohedral or orthorhombic symmetry because *A* ions cause a tilting of BO_6 octahedra in order to optimize A–O bonding. Perovskite oxides can be thought of consisting alternating BO_2 and A–O layers stacked over one another in <001> direction.

In principle, perovskite oxides can be categorized into five types on the basis of valencies *m* and *n* of cations *A* and *B*, respectively in ABO_3 [Galasso, (1969)]. The only criterion is that the sum of the valencies (m+n) of the cations must be equal to that of anions to

maintain charge neutrality. On the basis of this criterion, *A* ions may be chosen from the first, second and third group of the periodic table, and *B* ions from the fifth, fourth and third group of the periodic table, respectively [Wainer and Wentworth (1952)]. No tetravalent or pentavalent ion on A-site has been known to stabilize the perovskite structure. Therefore, there are only three categories of perovskite oxides, which actually exist.

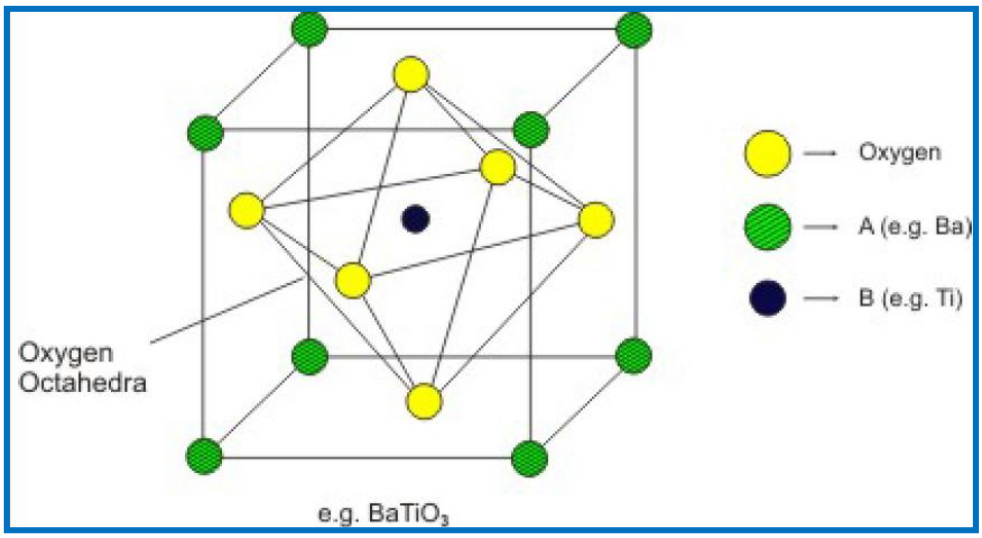

Figure 1.3 Perovskite structure

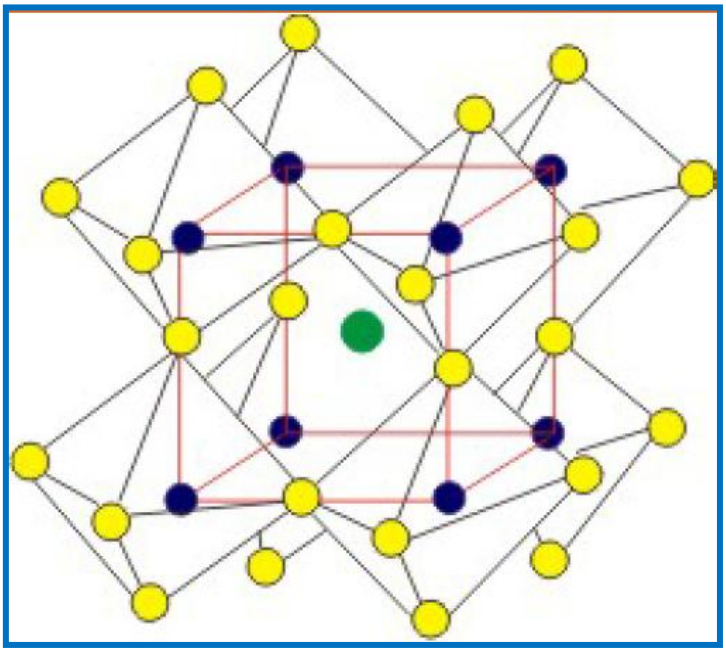

Figure 1.4 Polyhedra model of perovskite structure

The three categories of perovskite oxides are, therefore, the following:

(i) The cation *A* belongs to first group and cation *B* belong to the fifth group of the periodic table. Some important perovskite oxides of the type $A^{1+}B^{5+}O_3$ are $LiNbO_3$, $KNbO_3$, $AgNbO_3$, $NaTaO_3$, $AgTaO_3$ and $KTaO_3$. Most of the compounds of this type are either ferroelectric or anti-ferroelectric [Matthias (1949)]. Because of their large acoustic-optic and electro-optic coefficients at room temperature, many of these compounds like $LiNbO_3$, $LiTaO_3$ and $KTaO_3$ are used in electro-optic devices [Yamaoka and Matsui (1981)]. $KNbO_3$ finds application as second harmonic generator and $LiNbO_3$ is used as a switch [Roy et al. (1993)].

(ii) The cation *A* belongs to second group and cation *B* belongs to fourth group of periodic table. Some examples of this group are $A^{2+}B^{4+}O_3$ where *A* is a divalent ion (Ca, Sr, Ba or Pb) and *B* is a tetravalent ion (Ti, Zr or Sn). Among these perovskites, the most widely studied materials are $MTiO_3$ where M = Ba, Sr, Ca and Pb. These are used as dielectric and piezoelectric materials. Besides these conventional uses, this group of perovskite ceramics finds applications in the design of thermistors, sensors, phase shifters and resonator antennas [Funayama et al. (1989); Jaffe et al. (1971); Lines and Glass (1977)].

Perovskite compounds $CaTiO_3$ and $SrTiO_3$ after suitable modification become technologically important electro-ceramic and hence are widely used as dielectric thermistors and barrier layer capacitors (BLC). The properties of their grain boundaries interface [Yamaoka and Matsui (1981)]. Titanates of barium and lead exhibit piezoelectric as well as ferroelectric properties at room temperature. This makes them useful for large number of applications such as piezoelectric transducers, air transducers, gas lighter elements, dynamic and blast gauges and accelerometers, wave filters and high voltage sensors. They are useful for sound transmission, reception, ultrasonic cleaning

devices, information storage in computers, dielectric amplifiers and dielectric resonator antennas [Haertling (1986); Herbert (1985); Jaffe et al. (1971); Levinson (1988); Lines and Glass (1977); Roy et al. (1993)].

(iii) Cations *A* and *B* both belong to the third group of the periodic table. The compounds belonging to this category have a rare earth or yttrium ion on *A* site and a trivalent transition metal ion on *B* site i.e. $A^{3+}B^{3+}O_3$ type oxides. These are of particular interest for technical application as functional materials in many fields because of their interesting properties, such as mixed conductivity by both ions and electrons or holes migration [Goodenough (1974)]. Such materials can be employed in solid electrolyte fuel cells [Minh (1993)], as electrode materials, for oxygen sensing [Alcock et al. (1992)] and as humidity sensors [Lukaszewicz (1991)].

Alkaline earth titanate perovskites

Calcium titanate is a paraelectric material with distorted cubic structure [Kay and Bailey (1957)]. It has been reported that cacium titanate has an orthorhombic symmetry at room temperature and the structure becomes tetragonal at 600 °C which changes to cubic at 1000 °C.

In recent years, $SrTiO_3$ has attracted much attention for its potential applications, such as a substrate for epitaxial growth of high temperature superconductor thin films, in photolysis of water, as an oxygen sensor and in magneto hydrodynamic operations [Butler et al. (1981)], as photo-chromic and cathode-chromic materials, which are also used in memory devices, optical processors etc. [Bernay and Cowan (1981)].

$BaTiO_3$ is one of the most important materials in the family of alkaline earth titanate. In $BaTiO_3$, both barium and oxygen ions have radii of about 1.40 Å and together they make up a face centered cubic array. Octahedrally coordinated titanium ions located at B-sites,

the body centre of a perovskite unit cell, are the active ions promoting ferroelectricity. The low lying d-orbital of titanium leads to an eccentric atomic arrangement and large electrical polarizibility. On cooling from high temperature, $BaTiO_3$ undergoes three ferro-electric phase transitions. All the three transitions are displacive in nature involving atomic movements of 0.1 Å or less. The direction of spontaneous polarization changes from one ferroelectric phase to another. At temperature above 1450℃, it exists in the cubic form which is paraelectric. At room temperature, $BaTiO_3$ is tetragonal with axial ratio c/a ≈1.012 [Jaffe et al. (1971)]. The polymorphic phase transitions at lower temperatures are found to occur as:

$$\text{Cubic} \xrightarrow{130℃} \text{tetragonal} \xrightarrow{0℃} \text{orthorhombic} \xrightarrow{-90℃} \text{rhombohedral}$$

with the direction of spontaneous polarization Ps as $< 111 >$, $< 110 >$ and $< 001 >$ in rhombohedral, orthorhombic and tetragonal structure, respectively.

In recent years, perovskite ceramics have received great attention due to their vast applications in the magneto-electronic devices, solid oxide fuel cells, phase shifters and other microelectronic components [Sebastian (2008); Lekshmi et al. (2018); Coronado et al. (2014)]. Barium strontium titanate (BST) ceramic is one of the best examples of perovskite ceramics which possess excellent properties such as high dielectric constant, low dielectric loss, high breakdown field strength, high tunability (non-linear dielectric behaviour under bias electric field), tunable transition temperature (by varying the Ba/Sr ratio) and better mechanical and thermal responses. Because of its temperature dependent ferroelectric and paraelectric nature, it is extensively used in the design of capacitors, thermistors, oscillators, phase shifters, transducers, tunable filters, dielectric resonator antennas, sensors, dielectric layer in electro-luminescent display devices and advance

memory devices [Brankovic et al. (2005)]. BST is a solid solution of $BaTiO_3$ and $SrTiO_3$. $BaTiO_3$ exhibits ferroelectric phase at room temperature, which changes to paraelectric phase above the transition temperature (Curie point) of 403K. On the other hand, $SrTiO_3$ has transition temperature down near to absolute zero [Zhang et al. (1998)]. In the BST solid solution, by varying the ratio of Ba/Sr, Curie temperature varies linearly with increasing fraction of Sr [Vargas-Ortíz et al. (2012)]. Ceramic materials with low loss and monotonic dependence of dielectric constant on temperature are required for tunable microwave applications. Ferroelectric state of BST exhibits high dielectric and hysteresis loss during DC tunability in the microwave range [Takasu (2000)]. Materials in the paraelectric phase can be preferably used to avoid fatigue and aging because of absence of ferroelectric domain switching for microwave devices. $Ba_{(1-x)}Sr_{(x)}TiO_3$ materials with $x \geq 0.4$ has transition temperature below room temperature [Jeon (2004); Alexandru et al. (2006); Yu et al. (2013)] and therefore is paraelectric at room temperature. $Ba_{0.5}Sr_{0.5}TiO_3$ (BST0) has perovskite structure with Curie temperature below room temperature. It undergoes three different phase transitions similar to $BaTiO_3$ (cubic-tetragonal-orthorhombic-rhombohedral) but the transitions are shifted to lower temperatures. Only cubic structure is paraelectric and all other structures are ferroelectric [Jona and Shirane (1993)].

1.8 Liquid Phase Sintering

Perovskite ceramics with low sintering temperatures are in great demand for manufacturing of next generation low cost ceramic products such as substrates, multi-chip modules, micro-electro mechanical systems (MEMS), micro-opto-electro mechanical systems (MOEMS) and microwave components/devices [Tagantsev et al. (2013); Sherman et al. (2006); Maiti et al. (2006); Varghese et al. (2018); Joseph et al. (2018)]. A

ceramic material with low sintering temperature reduces the manufacturing cost. Controlled sintering conditions and effective sintering aid reduce sintering temperature and exaggerated grain growth. Several methods like chemical synthesis, high energy ball milling and liquid phase sintering are used for lowering the sintering temperature of ceramics [Varghese et al. (2016)]. Addition of low melting point glass to the ceramic to form a liquid phase (for liquid phase sintering) is one of the best methods for decreasing sintering temperature without degrading its properties [Rani and Sebastian(2008); Armstrong et al. (1990); Zhang et al. (2004)]. Homogeneously melted glass enhances the densification of ceramic at lower sintering temperatures. Liquid form of the glass penetrates the solid particle to spread uniformly and forms bridges between the grains. The capillary forces enhance compaction resulting in increase of its density. Besides acting as sintering aid, glasses also possess some inherent properties, such as low viscosity, high durability, low melting temperature and non-reactivity with the ceramic [Jeon et al. (2005)]. Multi-component glasses provide higher reduction in sintering temperature as well as better densification with good dielectric properties with respect to single component glass [Anjana and Sebastian (2009)]. Dielectric constant of glasses is stable within the microwave frequency range. Borosilicate glasses form –Si–O–B–O– linkages to give continuous atomic structure and possess low dielectric loss and high impedance [Bijumon and Sebastian (2005)]. $Bi_2O_3 - B_2O_3$ glasses provide large glass forming range with stable thermal and physical properties [Lee et al., (2005)]. The PbO in multi-component glass decreases the viscosity of melt, increases density and dielectric constant [Fujino et al. (2004)]. B_2O_3 content of glass plays important role by decreasing the viscosity and increasing densification and enhancing the release of free oxygen from the silicate structure. This weakens the network connectivity, which further results in the

reduction of melting point [Borhan et al. (2006)]. Khanna et al. (2014), and Wu and Huang (1999) have widely investigated the wide range of $PbO–B_2O_3–SiO_2$ glasses.

B_2O_3 is one of the most important glass formers incorporated into various kinds of ceramic systems as a flux and sintering aid. It was suggested that Bi_2O_3 can occupy both network forming and network modifying positions in the borate glasses. Therefore, the physical properties of such glasses exhibit continuous changes when the structural role of the cation is switched over from network forming to network modifying positions. On this basis, glasses containing Bi_2O_3 have attracted considerable attention due to their use as a flux, to lower the sintering temperature. Pyramid glass network [Wells (1975), Vogel (1985)] obtained after addition of small amount of Bi_2O_3 into B_2O_3 shows large glass forming range and stable physical and thermal properties [Shelby (1997); Varshneya (1994); Lee et al. (2005); Hoch (1996)]

In the present investigation, novel $60PbO–20B_2O_3–5BaO–15SiO_2$ (PBBS) glass and $55B_2O_3$-$45Bi_2O_3$ (BB) glass are synthesized and utilized as these are sintering aids to lower the sintering temperature of $Ba_{0.5}Sr_{0.5}TiO_3$ (BST) ceramic. The effects of PBBS and BB glass additions on the sintering temperature, phase and dielectric properties of BST ceramic are investigated comprehensively. Also, certain dielectric resonator antennas (DRAs) are designed using BST ceramics with appropriate percentage of PBBS and BB glass additions which meet the requirements of simpler structure, wide impedance bandwidth, reasonable gain and can achieve broadside or monopole like radiation pattern. The study primarily is focussed on the reduction of manufacturing cost and simpler DRA configurations with reduced material requirement.